LETTER

Acoustic emission enhancement and self-centering effect via an extreme anisotropic metamaterial

Applied Physics Express 16, 057002 (2023)
https://doi.org/10.35848/1882-0786/accfe2

LETTER

Acoustic emission enhancement and self-centering effect via an extreme anisotropic metamaterial

Yunzhong Lei, Jiu Hui Wu*, Libo Wang, Yao Huang, Shaokun Yang, and Jiamin Niu

School of Mechanical Engineering & State Key Laboratory for Strength and Vibration of Mechanical Structures, Xi'an Jiao Tong University, Xi'an 710049, People's Republic of China

*E-mail: ejhwu@xjtu.edu.cn

Received January 15, 2023; revised April 7, 2023; accepted April 24, 2023; published online May 9, 2023

An extreme anisotropic metamaterial consisting of one central cavity, eight zigzag and straight channels is proposed, aiming to achieve acoustic emission enhancement and self-centering effect. By placing a monopole source in the center of the metamaterial, acoustic emission enhancement can be achieved through the resonance in the zigzag channels and the monopole resonances. Theory and simulation confirm the self-centering effect of the proposed metamaterial, that is, when monopole sources are placed away from the center of the metamaterial, the external sound field can still be regarded as a uniform sound field generated by a monopole source placed in the center.

Supplementary material for this article is available online

Acoustic emission is one of the most fundamental topics in acoustics and has attracted increasing interest because of its importance in a variety of applications, such as sonar systems,[1] medical diagnostics,[2,3] and acoustic communication.[4,5] The radiated sound power of a monopole source is inversely proportional to the square of the wavelength and usually lower at low frequencies. Therefore, it is necessary to increase acoustic emissions. Horn is traditionally used to increase acoustic emissivity, which has a large size of the same order of magnitude as the wavelength and changes the radiation directionality of the monopole source. Phased array technology to modify the phase can eliminate interference between sound sources to achieve superposition enhancement, but the disadvantages are many electronic components and complex circuits. Fortunately, emerging acoustic metamaterials make these obstacles outdated.

Acoustic metamaterials are synthetic materials used to manipulate sound waves with properties that are almost impossible to achieve in nature, such as negative mass density and bulk modulus, double negative metamaterials, and extreme anisotropy.[6–11] Therefore, many acoustic metamaterial devices have been developed, such as subwavelength imaging systems,[12,13] acoustic magnifying hyperlens,[14–16] sound focusing,[17–19] and sound absorbers.[20,21] In terms of acoustic emission enhancement, a double-walled metamaterial structure provides efficient emission enhancement and changes the directionality of a unipolar source through Fabry–Perot resonance.[22] A space-coiling structure with an infinity effective mass density along the azimuth is used to enhance monochromatic multipole emission.[23,24] A simple "Lego" type acoustic metamaterial is proposed to increase the emissivity of monopole sources through the coupling between the resonances of a cavity and a dual grating.[25] A dual anisotropic metamaterial is employed to achieve enhanced broadband monopole emission via the coupling of the first and second monopole resonances.[26] Enhanced state density theory and radiation impedance theory are utilized to explain the mechanism of enhanced emission by metamaterial enclosures.[27,28] A subwavelength bianisotropic hybrid Mie resonator enables enhanced omnidirectional and directional antennas through monopole and dipole resonances, respectively.[29] It can be seen that most of the literature mainly achieves acoustic emission enhancement of centrally located monopole sources through anisotropic acoustic metamaterials with infinite mass density, and the potential of zero-mass density as another extreme mass density to enhance acoustic emission remains to be developed. Meanwhile, if the self-centering of monopole sources in metamaterial can be achieved, interference can be avoided, and the overlap of multiple monopole sources can be performed to further enhance emission.

Based on the above, the purpose of this letter is to introduce a new method to achieve enhanced acoustic emission and self-centering effect. To obtain satisfactory results, an extreme anisotropic metamaterial composed of one central cavity, eight zigzag and straight channels is proposed. Finite element simulation shows that multiple enhancement peaks occur when a monopole source is placed in the center of the extreme anisotropic metamaterial. The resonances corresponding to the enhancement peaks are investigated thoroughly, and the mechanism of emission enhancement is explained by radiation impedance theory. Then, it is theoretically derived that extreme anisotropic metamaterial can achieve the self-centering effect of monopole sources, and the simulation results confirm the theoretical analysis.

Figure 1(a) shows the schematic diagram of the proposed two-dimensional extreme anisotropic metamaterial, which has eight more lateral symmetrical zigzag channels than the traditional circular sound grid shown in Fig. 1(b). The significance of introducing the lateral zigzag channels is the effective mass density along the azimuth direction at the resonant frequency of the zigzag channels is zero.[30,31] In contrast, the effective mass density at other frequencies can be considered infinite. The radius of the central cavity is $R_1 = 60$ mm, the wall thickness is $t = 1$ mm, and the widths of the straight and zigzag channels are $d = 6$ mm and $w = 5$ mm, respectively. The "Pressure-Acoustic" module and "Acoustic-Thermo-viscous Acoustic Interaction" module in the finite element software (COMSOL Multiphysics) are used to investigate the radiation characteristic of a monopole source with a given surface velocity when it is placed in the center of the anisotropic metamaterial. We set background air with mass density $\rho_0 = 1.29\ \mathrm{kg\,m^{-3}}$ and sound velocity $c_0 = 340\ \mathrm{m\,s^{-1}}$. The perfectly match layer is placed at the outer boundary of the air domain to meet far-field conditions by eliminating

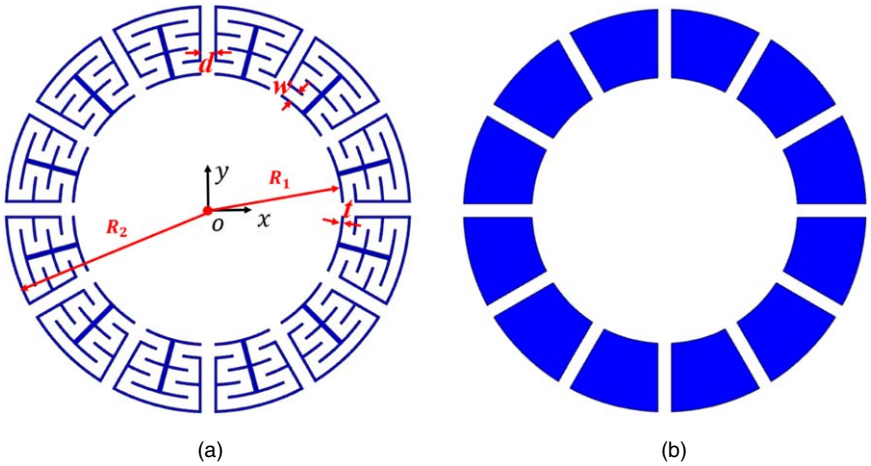

Fig. 1. Schematic diagrams of the proposed extreme anisotropic metamaterial (a) and traditional circular sound grid (b).

reflections. The frameworks of the anisotropic metamaterial are set to hard sound field boundaries.

The ratio of the radiated sound power P_1 of the monopole source in the presence of the extreme anisotropic metamaterial and the radiated sound power P_0 in free space is used to measure the enhanced efficiency. Where the radiated sound power P_1 and P_0 are obtained by integrating the sound energy flux on a cylindrical surface at a distance of 1 meter. The simulation results are shown in Fig. 2. The black and red lines represent the function of P_1/P_0 as a function of frequency when the anisotropic metamaterial has or does not have zigzag channels regardless of the thermos-viscous dissipation, respectively. P_1/P_0 as a function of frequency when considering the thermos-viscous dissipation and the anisotropic metamaterial with zigzag channels is plotted with the blue line. It can be seen from the black and red lines that when the anisotropic metamaterial with zigzag channels exists, three enhancement peaks appear at 480 Hz, 1347 Hz, and 3016 Hz, respectively, and $P_1/P_0 > 1$ occurs in three frequency ranges of 100–648 Hz, 1335–1363 Hz, and 2948–3084 Hz. When considering the thermos-viscous dissipation, the frequencies corresponding to the three enhancement peaks decrease to 464 Hz, 1315 Hz, and 2950 Hz, respectively. Although the second enhancement peak drops significantly, it still has similar efficiency to the other two peaks, indicating that the second enhancement peak has acoustic emission enhancement performance despite being severely affected by the thermos-viscous dissipation. However, when the anisotropic metamaterial does not have zigzag channels, there are only two enhancement peaks at 634 Hz and 3372 Hz, respectively, and P_1/P_0 is greater than 1 in the frequency ranges of 100–850 Hz and 3234–3532 Hz. It indicates that compared with the monopole resonances in the traditional circular sound grid, the proposed extreme anisotropic metamaterial has a new resonance mode to enhance acoustic emission.

Next, the normalized sound pressure diagrams in the metamaterial at each frequency corresponding to the enhancement peaks are further investigated to analyze the corresponding resonance modes, and the results are plotted in Fig. 3. Among them, Figs. 3(a)–3(c) are the sound pressure diagrams corresponding to the three enhancement peaks in the proposed anisotropic metamaterial, and the sound

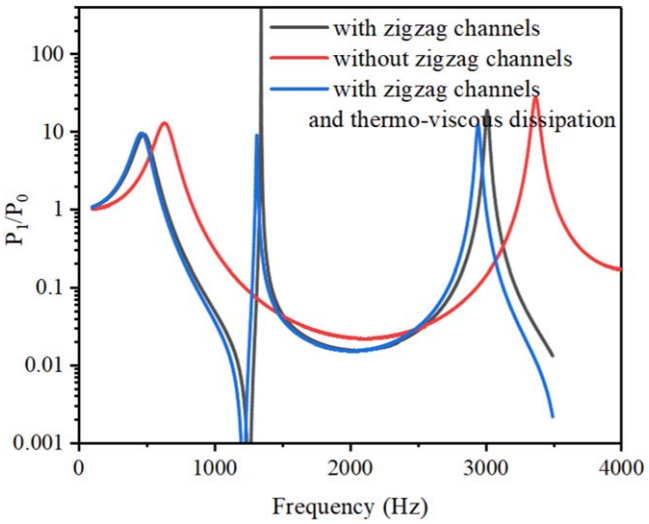

Fig. 2. The function of P_1/P_0 as a function of frequency when the anisotropic metamaterial has or does not have zigzag channels, respectively.

pressure diagrams of Figs. 3(d)–3(e) correspond to the two enhancement peaks in the traditional circular sound grid. It can be seen from Figs. 3(a) and 3(d) the enhanced peaks at 480 Hz and 634 Hz correspond to the first monopole resonance because the sound pressure is evenly distributed in all directions, and the amplitude is positive. In Figs. 3(c) and 3(e), although the sound pressure is still evenly distributed in all directions, the internal amplitude is positive, and the external amplitude is negative, so the enhanced peaks at 3016 Hz and 3372 Hz correspond to the second monopole resonance. Compared to Fig. 3(a), the sound pressure distribution in the central cavity and straight channels in Fig. 3(b) is consistent, but the amplitude of sound pressure in the zigzag channels changes from positive to negative, indicating that the resonance only occurs in the zigzag channels. When the resonance generates in the zigzag channels, the effective mass density along the azimuth direction is zero. In addition, at non-resonant frequencies, sound waves cannot pass through the zigzag channels, and the effective mass density along the azimuth direction can be regarded as infinity, like the traditional circular sound grid. In summary, the resonances of the proposed metamaterial in the case of two extreme anisotropies achieve acoustic emission enhancement, that is, the resonance in the zigzag channels

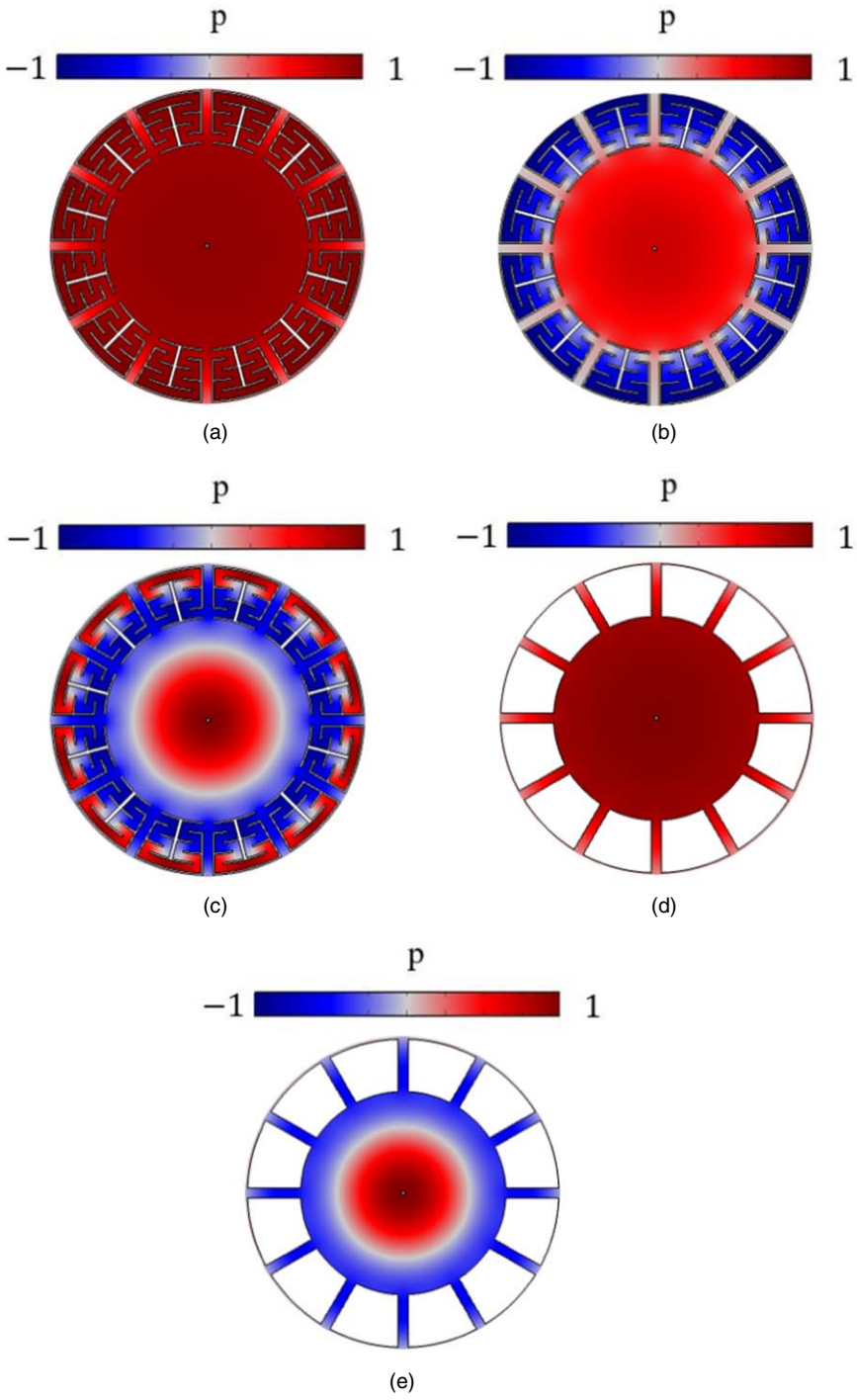

Fig. 3. (a)–(c) The sound pressure diagrams corresponding to the three enhancement peaks in the proposed anisotropic metamaterial. (d)–(e) The sound pressure diagrams corresponding to the two enhancement peaks in the traditional circular sound grid.

when the effective mass density is 0 along the azimuth direction and the monopole resonances in the entire metamaterial when the effective mass density is infinite along the azimuth direction.

In acoustic theory, for a monopole source with the given surface velocity U_0, the radiated sound power is determined only by radiation resistance Re(Z) because $P = U_0^2\mathrm{Re}(Z)/2$. The above analysis shows that the extreme anisotropic metamaterial changes the external environment of the monopole source through the monopole resonances and the resonance in the zigzag channels and then increases the radiation resistance to achieve the purpose of acoustic emission enhancement. To verify the above, the ratio of radiation resistances and radiated sound powers of the monopole source in the metamaterial and free space are calculated by numerical simulation, respectively, the results are shown in Fig. 4. The solid red line and the blue circle represent P_1/P_0 and $\mathrm{Re}(Z_1)/\mathrm{Re}(Z_0)$, respectively. The two curves fit perfectly. Therefore, the simulation results further confirm the mechanism of acoustic emission enhancement of the extreme anisotropic metamaterial. Furthermore, the effects of the critical parameters on acoustic emission enhancement are investigated thoroughly (Supplementary Note 1).

The theory is used to analyze how monopole sources self-centering in the extreme anisotropic metamaterial are

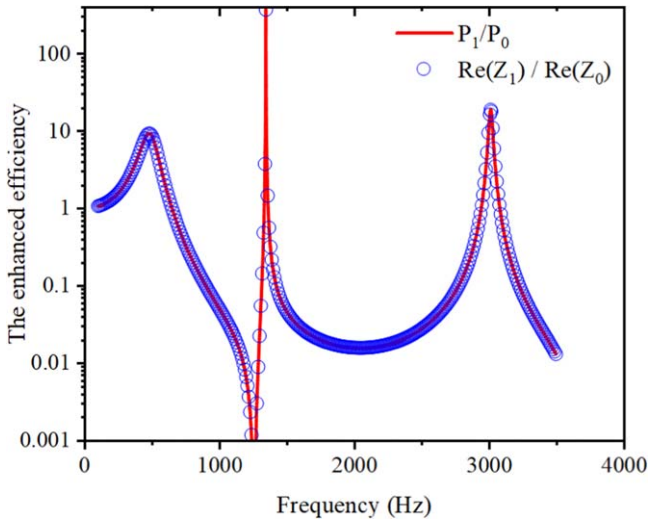

Fig. 4. The solid red line and the blue circle represent P_1/P_0 and $\mathrm{Re}(Z_1)/\mathrm{Re}(Z_0)$, respectively.

achieved when the effective mass density along the azimuth is zero and infinity. For a monopole source with radius a and the given surface velocity of U_0, the amplitude of the sound pressure is $P = \frac{-i\rho_0 c_0}{H_1(k_0 a)} U_0 H_0(k_0 a)$. $H_0(k_0 a)$ and $H_1(k_0 a)$ are the Hankel function of the first kind, and wave number $k_0 = \omega/c_0$. Next, we will derive the pressure field and radial velocity of each region shown in Fig. 1 to obtain the sound pressure field outside the metamaterial. In the central cavity ($r < R_1$):

$$p_1 = \sum_{n=0}^{\infty} A_n J_n(k_0 r)\cos(n\theta) + \frac{-i\rho_0 c_0}{H_1(k_0 a)} U_0 \sum_{m=-\infty}^{m=\infty} J_m(k_0 r_1) H_m(k_0 r) e^{im(\theta-\theta_1)} \quad (1)$$

$$v_{r1} = \frac{1}{i\omega\rho_0}\left[\sum_{n=0}^{\infty} A_n J_n'(k_0 r)\cos(n\theta) + \frac{-i\rho_0 c_0}{H_1(k_0 a)} U_0 \sum_{m=-\infty}^{m=\infty} J_m(k_0 r_1) H_m'(k_0 r) e^{im(\theta-\theta_1)}\right], \quad (2)$$

where $J_n(k_0 r)$ is the Bessel function. r_1 and θ_1 represent the vector distance of the monopole source from the origin in the coordinate system with the metamaterial center as the origin. When ($R_1 < r < R_2$):

$$p_2 = \sum_{n=0}^{\infty} [B_n J_v(k_r r) + C_n H_v(k_r r)]\cos(n\theta) \quad (3)$$

$$v_{r2} = \frac{1}{i\omega\rho_r}\sum_{n=0}^{\infty} [B_n J_v'(k_r r) + C_n H_v'(k_r r)]\cos(n\theta) \quad (4)$$

Where $v = n\sqrt{\rho_r/\rho_\theta}$ and $k_r = \omega\sqrt{\rho_r/\kappa}$. Outside the metamaterial ($r < R_2$):

$$p_3 = \sum_{n=0}^{\infty} D_n H_n(k_0 r)\cos(n\theta) \quad (5)$$

$$v_{r3} = \frac{1}{i\omega\rho_0}\sum_{n=0}^{\infty} D_n H_n'(k_0 r)\cos(n\theta). \quad (6)$$

In Eqs. (1)–(6), A_n, B_n, C_n and D_n are unknown coefficients. When ρ_θ is 0, for v to make sense, n in Eqs. (3)–(4) can only be 0. It shows that the sound pressure field and velocity field in the region of $R_1 < r < R_2$ are independent of θ. Meanwhile, to meet the continuous boundary conditions, the sound pressure field and velocity field in other regions should also be independent of θ, that is, n and m in Eqs. (1)–(6) are 0. Therefore, the above equations can be simplified as:

$$p_1 = A_0 J_0(k_0 r) + \frac{-i\rho_0 c_0}{H_1(k_0 a)} U_0 J_0(k_0 r_1) H_0(k_0 r) \quad (7)$$

$$v_{r1} = \frac{1}{i\omega\rho_0}\left[A_0 J_0'(k_0 r) + \frac{-i\rho_0 c_0}{H_1(k_0 a)} U_0 J_0(k_0 r_1) H_0'(k_0 r)\right] \quad (8)$$

$$p_2 = B_0 J_0(k_r r) + C_0 H_0(k_r r) \quad (9)$$

$$v_{r2} = \frac{1}{i\omega\rho_r}[B_0 J_0'(k_r r) + C_0 H_0'(k_r r)] \quad (10)$$

$$p_3 = D_0 H_0(k_0 r) \quad (11)$$

$$v_{r3} = \frac{1}{i\omega\rho_0} D_0 H_0'(k_0 r). \quad (12)$$

Similarly, when ρ_θ is infinity, $v = n\sqrt{\rho_r/\rho_\theta} \approx 0$. Since the monopole resonances correspond to $n = 0$, Eqs. (1)–(6) are also simplified as to Eqs. (7)–(12). According to the continuous sound pressure field and velocity field at the interface of $r = R_1$ and $r = R_2$, $p_3 = \frac{-i\rho_0 c_0}{H_1(k_0 a)} U_0 J_0(k_0 r_1)\frac{T_1}{T_2} H_0(k_0 r)$ can be obtained. Where:

$$T_1 = \begin{bmatrix} J_0(k_0 R_1) & -J_0(k_r R_1) & -H_0(k_r R_1) & -H_0(k_0 R_1) \\ \frac{1}{j\omega\rho_0} J_0'(k_0 R_1) & -\frac{1}{j\omega\rho_r} J_0'(k_r R_1) & -\frac{1}{j\omega\rho_r} H_0'(k_r R_1) & -\frac{1}{j\omega\rho_0} H_0'(k_0 R_1) \\ 0 & J_0(k_r R_2) & H_0(k_r R_2) & 0 \\ 0 & \frac{1}{j\omega\rho_r} J_0'(k_r R_2) & \frac{1}{j\omega\rho_r} H_0'(k_r R_2) & 0 \end{bmatrix}$$

$$T_2 = \begin{bmatrix} J_0(k_0 R_1) & -J_0(k_r R_1) & -H_0(k_r R_1) & 0 \\ \frac{1}{j\omega\rho_0} J_0'(k_0 R_1) & -\frac{1}{j\omega\rho_r} J_0'(k_r R_1) & -\frac{1}{j\omega\rho_r} H_0'(k_r R_1) & 0 \\ 0 & J_0(k_r R_2) & H_0(k_r R_2) & -H_0(k_0 R_2) \\ 0 & \frac{1}{j\omega\rho_r} J_0'(k_r R_2) & \frac{1}{j\omega\rho_r} H_0'(k_r R_2) & -\frac{1}{j\omega\rho_0} H_0'(k_0 R_2) \end{bmatrix}.$$

It can be seen that the sound pressure field outside the metamaterial is independent of r_1 and θ_1, which indicates that the self-centering effect exists in the following two cases: the effective mass density along the azimuth direction is zero and the monopole resonances occur when the effective mass density is infinite. The self-centering effect is when the monopole source is placed anywhere in the central cavity, the external sound field appears to be emitted from the center of the metamaterial.

When there are multiple monopole sources in the central cavity, $p_3 = \sum_{f=1}^{g} \frac{-i\rho_0 c_0}{H_1(k_0 a_f)} U_f J_0(k_0 r_f) \frac{T_1}{T_2} H_0(k_0 r)$, where g is the number of monopole sources, and a_f, U_f, and r_f are the radius, surface velocity, and distance from the center, respectively. The external sound pressure field distribution can be regarded as the result of overlapping emission of multiple monopole sources in the center without interference, which is beneficial to further enhance the acoustic emission.

Next, the finite element simulation is performed to verify the above theoretical analysis. Two monopole sources are placed in $(0.2\lambda, 0)$ and $(-0.2\lambda, 0)$, respectively, where λ is the wavelength. The sound pressure diagrams at the frequencies of 1347 Hz and 3016 Hz in the presence or absence of extreme anisotropic metamaterial are plotted in Fig. 5. It can be seen in Figs. 5(a) and 5(c) that two monopole sources with a distance of 0.4λ will have significant interference in free space to produce an inhomogeneous sound field. However, when the extreme anisotropic metamaterial is present, the outer sound pressure field becomes uniform and can be regarded as a circular wave. Compared with the sound pressure field in free space, the sound pressure field in the presence of extreme anisotropic metamaterial is significantly enhanced.

To more accurately demonstrate the performance of extreme anisotropic acoustic metamaterial, the sound pressure levels (SPLs) in the orthogonal direction and on a circle with a radius of 2λ at the frequencies of 1347 Hz and 3016 Hz in the presence or absence of extreme anisotropic metamaterial are plotted in Figs. 6 and 7, respectively. In Fig. 6, the black and red lines indicate SPLs as the function of d/λ in the orthogonal direction of free space, respectively. There is a significant difference in SPLs in the x and y directions due to interference. However, when the extreme anisotropic metamaterial exists, the SPLs in the x and y directions are almost the same and are higher than the SPLs in free space, which can be seen from the blue line and the green circle. The blue lines in Fig. 7 represent the SPL distribution on the circle of radius 2λ in free space, which are dipole distributions due to the interference between two monopole sources. When the extreme anisotropic metamaterial exists, it can be seen from the red lines that the SPLs are consistent along the azimuth and higher than the SPLs in free space. The phenomenon further indicates that the proposed metamaterial has the self-centering effect to make multiple monopole sources overlap in the center without interference. To demonstrate the presence of the self-centering effect of the monopole sources at any positions in the central cavity of the proposed metamaterial, the corresponding results with other source positions are provided (Supplementary Note 2).

In conclusion, an extreme anisotropic metamaterial composed of one central cavity, eight zigzag and straight channels is proposed to achieve acoustic emission enhancement and self-centering effect. Extreme anisotropy manifests as the effective mass density along the azimuth direction at the resonant frequency of the zigzag channels is zero, and can be considered infinite at other frequencies. Based on radiation impedance theory and simulation analysis, the mechanism of enhanced acoustic emission is to change the external environment of the monopole source through the monopole resonances and the resonance in the zigzag channels and then increase the radiation resistance. The mechanism by which the extreme anisotropic metamaterial achieves a self-centering effect makes multiple monopole sources overlap in the center without interference in the following two cases is derived theoretically, that is, the effective mass density along

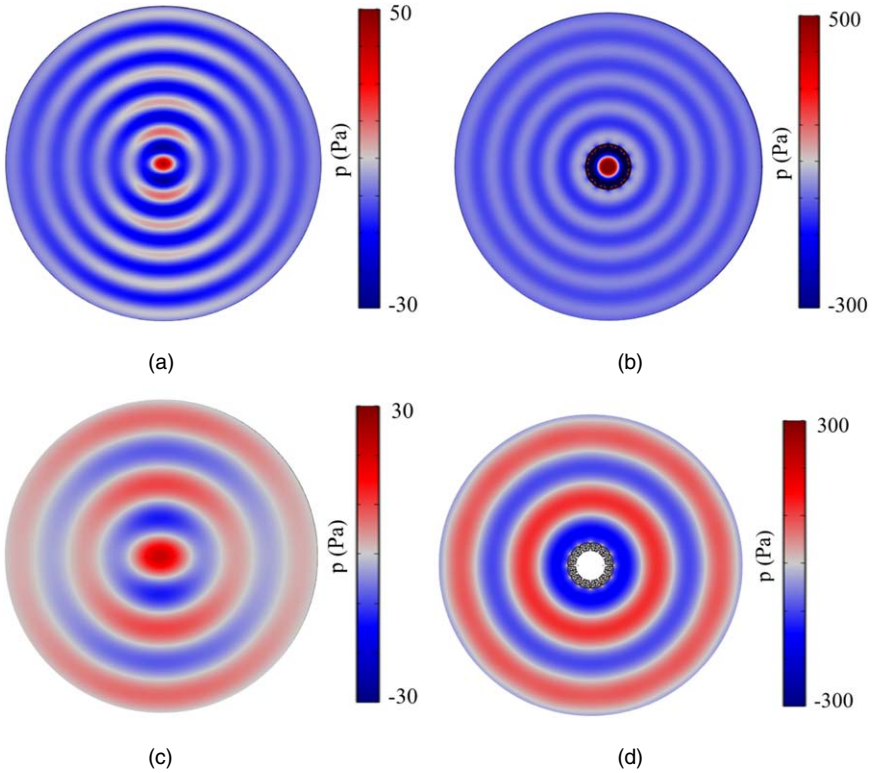

Fig. 5. (a)–(b) Sound pressure diagrams in free space and the presence of the extreme anisotropic metamaterial at 1347 Hz. (c)–(d) Sound pressure diagrams in free space and the presence of the extreme anisotropic metamaterial at 3016 Hz.

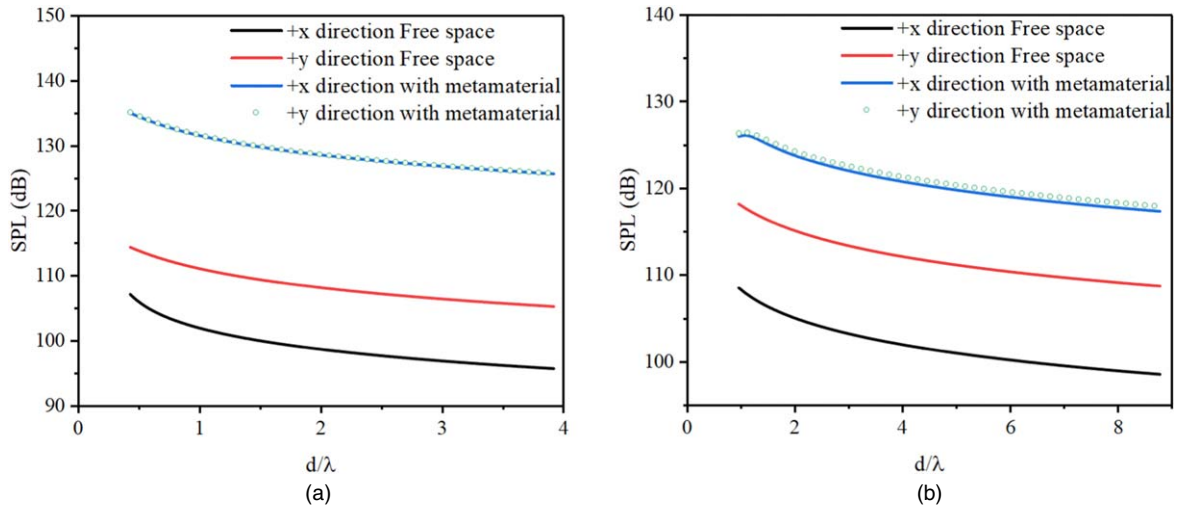

Fig. 6. (a) The SPLs in the orthogonal direction at 1347 Hz. (b) The SPLs in the orthogonal direction at 3016 Hz.

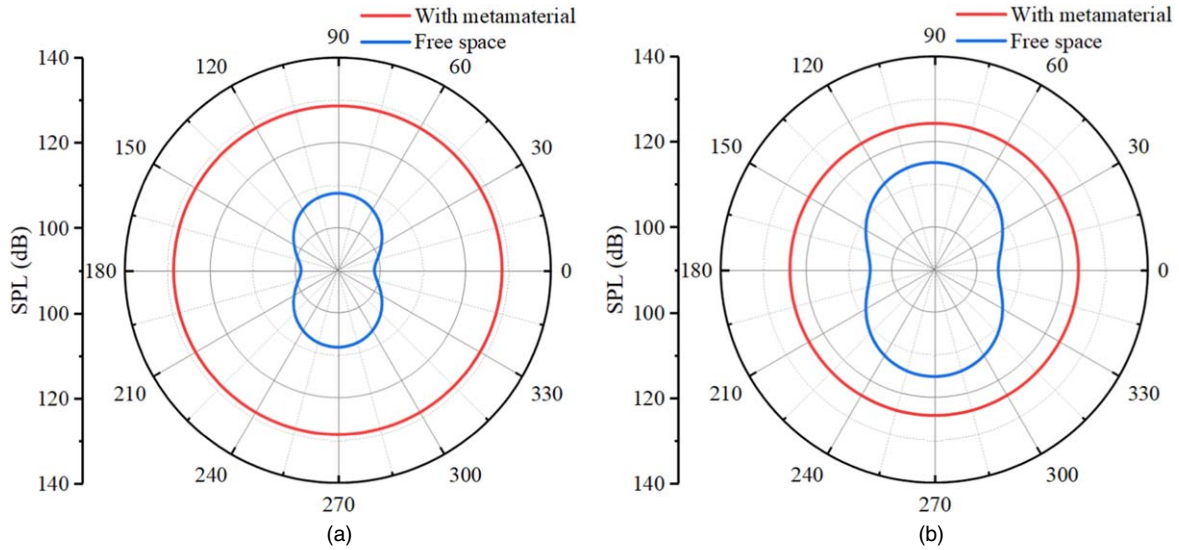

Fig. 7. The SPLs on a circle with a radius of 2λ at 1347 Hz (a) and 3016 Hz (b), respectively.

the azimuth direction is zero and the monopole resonances occur when the effective mass density is infinite. The sound pressure field and the SPLs obtained by simulation in the orthogonal direction and on the circle with a radius of 2λ show a significant difference due to the inhomogeneous sound field generated by interference in free space. However, when the metamaterial exists, the external sound pressure field becomes uniform, which can be regarded as a circular wave, and the SPLs in the orthogonal direction and on the circle with a radius of 2λ are almost the same and higher than the SPLs in free space. The proposed extreme anisotropic metamaterial provides an alternative method for acoustic emission enhancement and self-centering effect, which may have potential application in acoustic communication.

Acknowledgments This work was supported by the National Natural Science Foundation of China (NSFC) under Grant No. 51675401.

ORCID iDs Libo Wang https://orcid.org/0000-0002-3016-0991

1) T. Josserand and J. Wolley, Ultrasonics **51**, 275 (2011).
2) A. P. Sarvazyan, M. W. Urban, and J. F. Greenleaf, Ultrasound Med. Biol. **39**, 1133 (2013).
3) O. Bucci, L. Crocco, R. Scapaticci, and G. Bellizzi, Proc. IEEE **104**, 633 (2016).
4) Z. Zhang, Y. Tian, Y. Wang, S. Gao, Y. Cheng, X. Liu, and J. Christensen, Adv. Mater. **30**, e1803229 (2018).
5) L. Freitag, M. Grund, S. Singh, J. Partan, P. Koski, and K. Ball, IEEE Proc. OCEANS 2005 MTS, 2005, **2**, p. 1086.
6) Z. Liu, X. Zhang, Y. Mao, Y. Y. Zhu, Z. Yang, C. T. Chan, and P. Sheng, Science **289**, 1734 (2000).
7) N. Fang, D. Xi, J. Xu, M. Ambati, W. Srituravanich, C. Sun, and X. Zhang, Nat. Mater. **5**, 452 (2006).
8) Y. Ding, Z. Liu, C. Qiu, and J. Shi, Phys. Rev. Lett. **99**, 093904 (2007).
9) J. Li and C. T. Chan, Phys. Rev. E **70**, 055602 (2004).
10) Y. Lai, Y. Wu, P. Sheng, and Z. Q. Zhang, Nat. Mater. **10**, 620 (2011).
11) Y. Chen, H. Liu, M. Reilly, H. Bae, and M. Yu, Nat. Commun. **5**, 5247 (2014).
12) H. Jia, M. Ke, R. Hao, Y. Ye, F. Liu, and Z. Liu, Appl. Phys. Lett. **97**, 173507 (2010).
13) J. Zhu, J. Christensen, J. Jung, L. Martin-Moreno, X. Yin, L. Fok, X. Zhang, and F. J. Garcia-Vidal, Nat. Phys. **7**, 52 (2011).
14) W. Wang, Y. Xie, A. Konneker, B.-I. Popa, and S. A. Cummer, Appl. Phys. Lett. **105**, 101904 (2014).
15) L. Zigoneanu, B.-I. Popa, and S. A. Cummer, Phys. Rev. B **84**, 024305 (2011).
16) J. Li, L. Fok, X. Yin, G. Bartal, and X. Zhang, Nat. Mater. **8**, 931 (2009).
17) J.-P. Xia, X.-T. Zhang, H.-X. Sun, S.-Q. Yuan, J. Qian, and Y. Ge, Phys. Rev. Appl. **10**, 014016 (2018).

18) S.-W. Fan, S.-D. Zhao, L. Cao, Y. Zhu, A. L. Chen, Y.-F. Wang, K. Donda, Y.-S. Wang, and B. Assouar, Phys. Rev. B **2**, 101 (2020).
19) S. Qi, Y. Li, and B. Assouar, Phys. Rev. Appl. **7**, 054006 (2017).
20) X. Peng, J. Ji, and Y. Jing, J. Acoust. Soc. Am. **144**, EL255 (2018).
21) S. Huang, X. Fang, X. Wang, B. Assouar, Q. Cheng, and Y. Li, J. Acoust. Soc. Am. **145**, 254 (2019).
22) K. Song, S. H. Lee, K. Kim, S. Hur, and J. Kimm, Sci. Rep. **4**, 4165 (2014).
23) J. Zhao, L. Zhang, and Y. Wu, J. Acoust. Soc. Am. **142**, EL24 (2017).
24) J. Zhao, R. A. Jahdali, L. Zhang, and Y. Wu, Sci. Rep. **8**, 1018 (2018).
25) J. Mei and Y. Wu, Sci. Rep. **9**, 11659 (2019).
26) Y. Lei, J. H. Wu, Z. Huang, and S. Yang, J. Phys. D: Appl. Phys. **55**, 065301 (2021).
27) F. Liu, W. Li, and M. Ke, Phys. Rev. Appl. **10**, 054031 (2018).
28) M. Landi, J. Zhao, W. E. Prather, Y. Wu, and L. Zhang, Phys. Rev. Lett. **120**, 114301 (2018).
29) Y. Jia, Y. Luo, D. Wu, Q. Wei, and X. Liu, Adv. Mater. Technol. **5**, 1900970 (2020).
30) Y. Li, B. Liang, X.-Y. Zou, and J.-C. Cheng, Appl. Phys. Lett. **103**, 063509 (2013).
31) Z. Liang and J. Li, Phys. Rev. Lett. **108**, 114301 (2012).